Offshore Wind Evidence + Change Programme

FLOWERS: WP1

Technical Appendix: Modelling Seabed Impacts of Floating Offshore Wind

Authors: David Haverson, Claire Beraud, Robert McEwan, Jennifer Graham, Jon Rees

Date: July 2025

THE CROWN ESTATE

Contents

Document Control

Version	Author	Checked	Approved	Date	Description of change

1. Introduction

The FLOWERS project forms part of the Offshore Wind Evidence and Change programme, led by The Crown Estate in partnership with the Department for Energy Security and Net Zero and Department for Environment, Food & Rural Affairs. The Offshore Wind Evidence and Change programme is an ambitious strategic research and data-led programme. Its aim is to facilitate the sustainable and coordinated expansion of offshore wind to help meet the UK's commitments to low carbon energy transition whilst supporting clean, healthy, productive and biologically diverse seas.

Renewable energy sources, such as wind energy, play an important role in the UK by providing clean energy to help decarbonise the UK's energy mix and aiding the UK Government's commitment to Net Zero greenhouse gas emissions by 2050. In 2020, wind power accounted for 24% of the total electricity generation in the UK and is growing, with offshore wind alone providing 13% (UK Government ONS, 2021). The UK is an ideal location for offshore wind, as shallow waters surround the entire coastline, but fixed offshore wind structures are typically limited to water depths up to 40 m (Sánchez et al., 2019). Floating wind turbines offer the opportunity to overcome this limitation, greatly increasing the potential for offshore wind energy in deeper waters, not only in the UK, but also globally.

Floating wind turbines will differ from fixed structures in terms of their structural design, as well as positioning in the marine environment. Therefore, work is needed to understand the potential impacts of these new developments on the marine ecosystem. This project aims to address one such impact: assessing potential disturbance resulting from mooring lines on the seabed. Different options exist for design of floating structures, including floating barges, semi-submersible platforms or spar-buoys that extend deeper into the water column. While some designs have proposed the use of taut lines to keep structures in place (e.g., tension-leg platforms), most to date use either slack or semi-taut catenary mooring lines (e.g., Watson et al., 2019; Jiang, 2025). As catenary moorings allow movement of the structure and lines, this may then cause abrasion and local scour, potentially changing the seabed composition and impacting the habitat of benthic species.

The aim of this research is to provide a methodology to assess such impacts, from the scale of individual mooring lines and floating structures up to wind farms and shelf-wide impacts. To do so, a suite of models have been developed, which combine detailed engineering models (OpenFAST) of floating wind turbine structure movements (Section 2) with the modelling capabilities of hydrodynamic models, such as TELEMAC (Section 3) and NEMO (Section 4), which both provide coupling to sediment transport. This provides an assessment of the potential interaction of structures with the seabed on different scales and predicts changes in sediment distribution and composition. These results have the potential to inform spatial planning, alongside tools such as OneBenthic (Cooper and Barry, 2017), to assess potential impacts on benthic marine ecosystems. However, they also highlight where further observations are needed to support model validation and impact assessment.

2. Mooring line impacts

2.1 Mechanisms for impact

Catenary mooring lines can be used to keep a floating wind turbine in place ('on station'), attached between the base of the floating structure and anchors on the seabed. This allows the floating structure to move freely under wind, waves and tidal current forcing, while remaining within a fixed zone. As well as the mooring line configuration, the width and depth of the floating platform, both above and below water, will determine how it moves under different environmental conditions (e.g., Jiang, 2025). While spar-buoys are common in deeper waters (depths > 100 m), here we focus on semi-submersible structures as those most likely to be deployed in shallower regions of interest around the UK. We chose a simple catenary design, suitable for the selected semi-submersible floating platform.

Depending on the motion of the floating structure, a varying portion of the mooring line will lie on the seabed (Figure 1 and Figure 2). The area of the seabed where the mooring line lies, known as the touch down zone (TDZ), will be physically abraded by the motion of the mooring line. Additionally the seabed in close vicinity to and along the line will experience scour due to an increased water velocity and turbulence. For clarity, hereafter we refer to both these combined effects of the mooring lines on the seabed as scour. The potential impact of mooring lines on the seabed will then depend on the design and movement of the floating wind structure.

There are three different mechanisms by which the structure and mooring lines may move. The first occurs when the floating platform moves off-station due to mean drift from wind, wave or tidal forcing, altering the tension of each mooring line, becoming taut or slack on different sides of the structure, depending on the direction of the forcing. The second occurs under higher frequency wave forcing, whereby bobbing of the platform causes the mooring lines to swing, generating localised turbulence near the bed, mobilising the sediments and leading to scour. Finally, in addition to movement of the platform, waves and tides can act directly on the mooring lines, causing drift as well as vortex-induced vibrations.

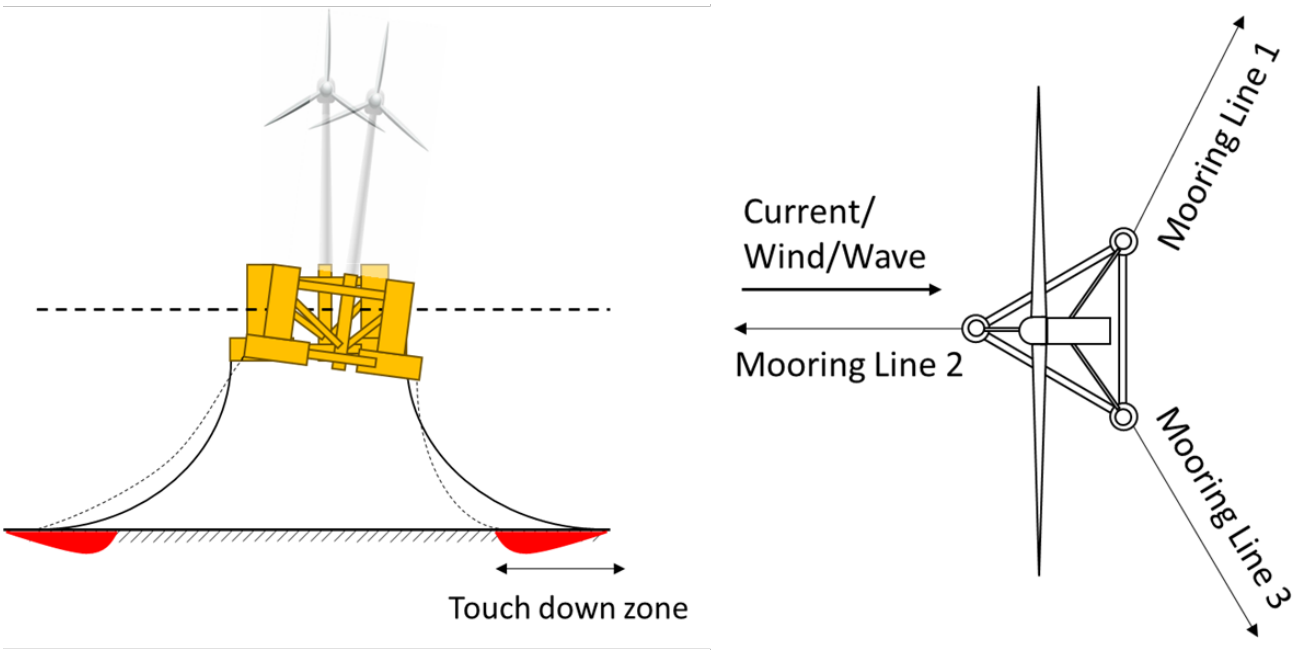

Figure 1. OC4-DeepCWind semi-submersible floating wind platform and mooring system, illustrating change in touch down zone under environmental forces.

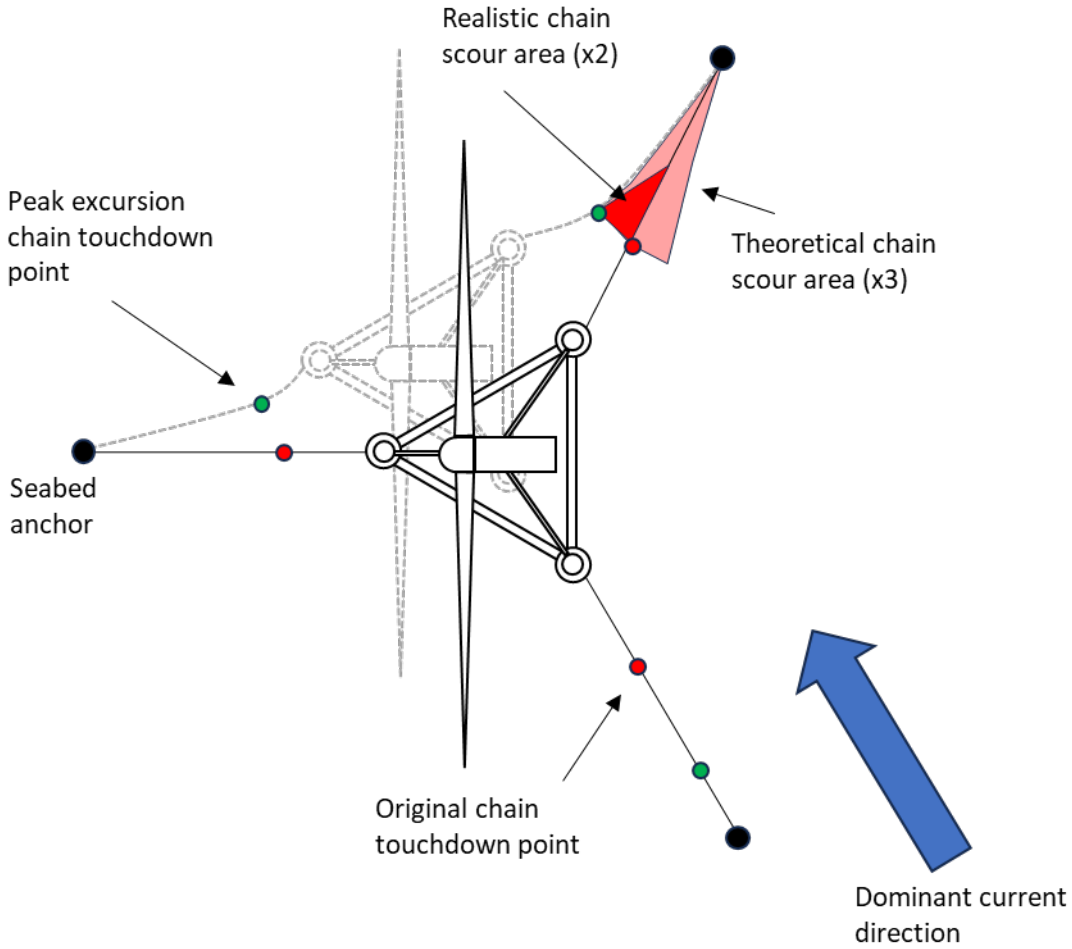

Figure 2. Illustration of the horizontal scour due to change in touch down zone under environmental forces.

2.2 OpenFAST model description

Engineering models have been developed to aid in the design and testing of floating wind turbines under various environmental conditions, primarily wind, waves, and currents. These models help to understand how these floating structures may move. However, assessing the environmental impact remains challenging, due to complex interactions between different processes.

To understand how the length of the TDZ (Touch Down Zone; Figure 1) per mooring line varies under different environmental conditions, a single wind turbine was modelled using OpenFAST[1] v3.3.0, an open-source aero-hydro-servo-elastic engineering model, developed by the National Renewable Energy Laboratory (NREL). OpenFAST simulates the heave, roll and pitch of the floating structure under winds, waves and currents, with the resulting forces and motions applied to the mooring lines.

Two different sizes of offshore wind turbine were investigated here, utilising publicly available OpenFAST model set ups: a NREL 5 MW turbine model[2] and an IEA 15 MW turbine model[3]. Both turbines incorporate semi-submersible floating platforms, and their associated mooring configurations within the publicly available model set ups, that are suited to UK shelf seas, specifically the OC4-DeepCWind design for the 5 MW turbine (Robertson et al., 2014) and the UMaine VolturnUS-S design for the 15 MW turbine (Allen et al., 2020). Key parameters for each simulation are summarised in Table 1.

Table 1. Floating wind turbine specifications considered in OpenFAST simulations.

Parameter	NREL 5 MW turbine	IEA 15 MW turbine
Rotor Diameter	128 m	240 m
Number of structure spurs	3	3
Spur diameters	12 m	12.5
Platform Draft	20 m	20 m
Number of mooring lines	3	3
Mooring line diameter	0.09 m	0.333 m
Mooring line mass	77.707 kg/m	685 kg/m
Water depth (for this study)	100 m	100 m

For both wind turbine sizes, the selected mooring system comprises three catenary lines, anchored to the seabed at one end and connected to the floating structure at three fairlead points, as shown in Figure 1. The simulations assumed untrenched mooring lines and a seabed without distinctive features. In this study, the mooring line length was set to 417.68 m to

[1] National Renewable Energy Laboratory OpenFAST model https://www.nrel.gov/wind/nwtc/openfast.html

[2] National Renewable Energy Laboratory 5 MW wind turbine https://github.com/ricklupton/OpenFAST-NREL-5MW.

[3] International Energy Agency 15 MW wind turbine https://github.com/IEAWindTask37/IEA-15-240-RWT.

accommodate the 100 m water depth of the study site, compared to the 200 m water depths assumed in the opensource OpenFAST setups. The MoorDyn module of OpenFAST was utilised to simulate the mooring line position, therefore allowing for calculation of the TDZ extent. Furthermore, the number of segments used to calculate line movement within the model was increased from 20 to 50, to enhance the representation of the mooring line and consequently the resolution of TDZ extent.

2.3 Study Site – Celtic Sea

For this project, the site selection was based on areas already identified for future floating wind farm development (4C Offshore, 2021). To ensure data availability (e.g., bathymetric and OneBenthic sediment characteristic data), the case study focussed on a location in the Celtic Sea (Figure 3). This site had also been considered during a previous modelling study that investigated the impact of wind turbines on benthic communities (Beraud et al., 2021).

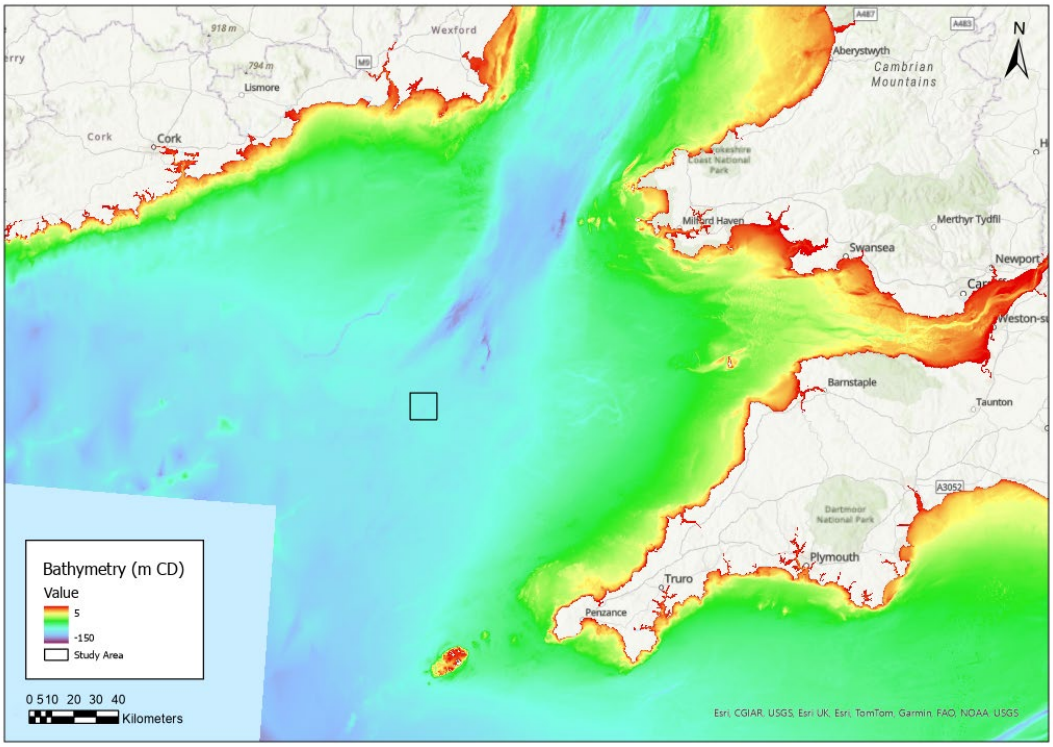

Figure 3. Map of the Celtic Sea, with shading showing bathymetry and black box showing location of the case study.

The average wave height at this location is approximately 1.9 metres, with wind speeds around 9 metres per second, predominantly from the west-southwest (Figure 4). The tidal current ellipse is oriented in a northeast-southwest direction, with a maximum current speed reaching 0.4 metres per second.

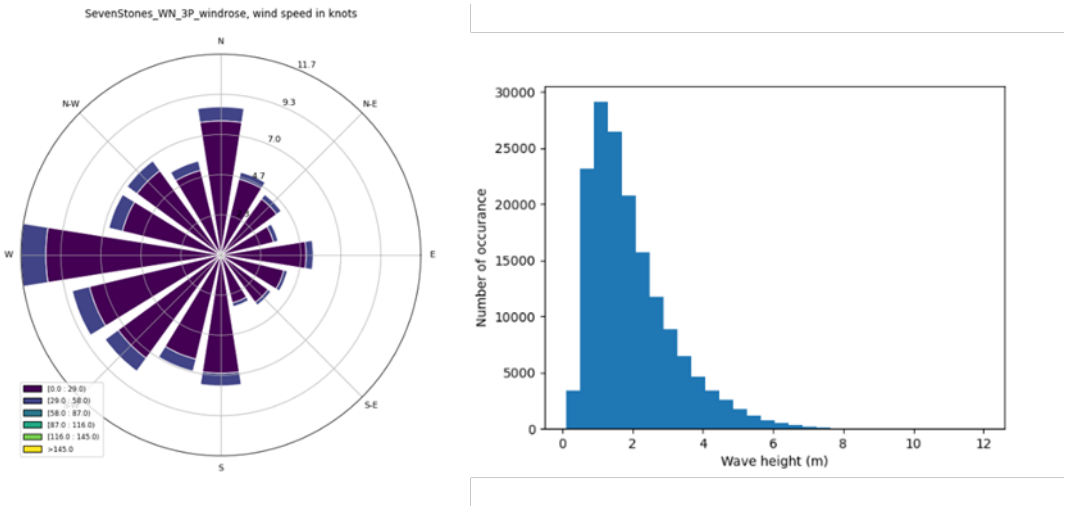

Figure 4. Left: Windrose from wind data; Right: wave heights occurrence. Data from Sevenstones Light Vessel station (WMO ID: 62107), measured between 2003 and 2022. Wind magnitude is displayed in knots and wave height in metres.

To investigate the motions of the mooring lines, the 5 MW and 15 MW models were then subjected to a range of wind speeds, wave heights and tidal currents that may be expected for the Celtic Sea. As the full envelope of possible combined impacts was prohibitive to fully investigate, the effects of wind, waves and currents were modelled separately. Wind speeds were incrementally tested between 0 – 20 m/s, wave heights between 0 – 12 m, and current speeds between 0 – 2 m/s.

2.4 OpenFAST model results

The results of the sensitivity testing showed that waves had little effect on the range of TDZ extents and that tidal currents exerted the greatest impact on the seabed (largest TDZ), followed by wind. Preliminary tidal direction analysis also identified 45 degrees (i.e., currents moving towards the northeast) as the most impactful direction. Figure 5 shows the full range of the mooring line positions for the 5 MW and 15 MW turbines, respectively, under tidal currents acting at 45 degrees. Further analysis focuses purely on this direction in relation to the mooring lines, as the worst-case scenario.

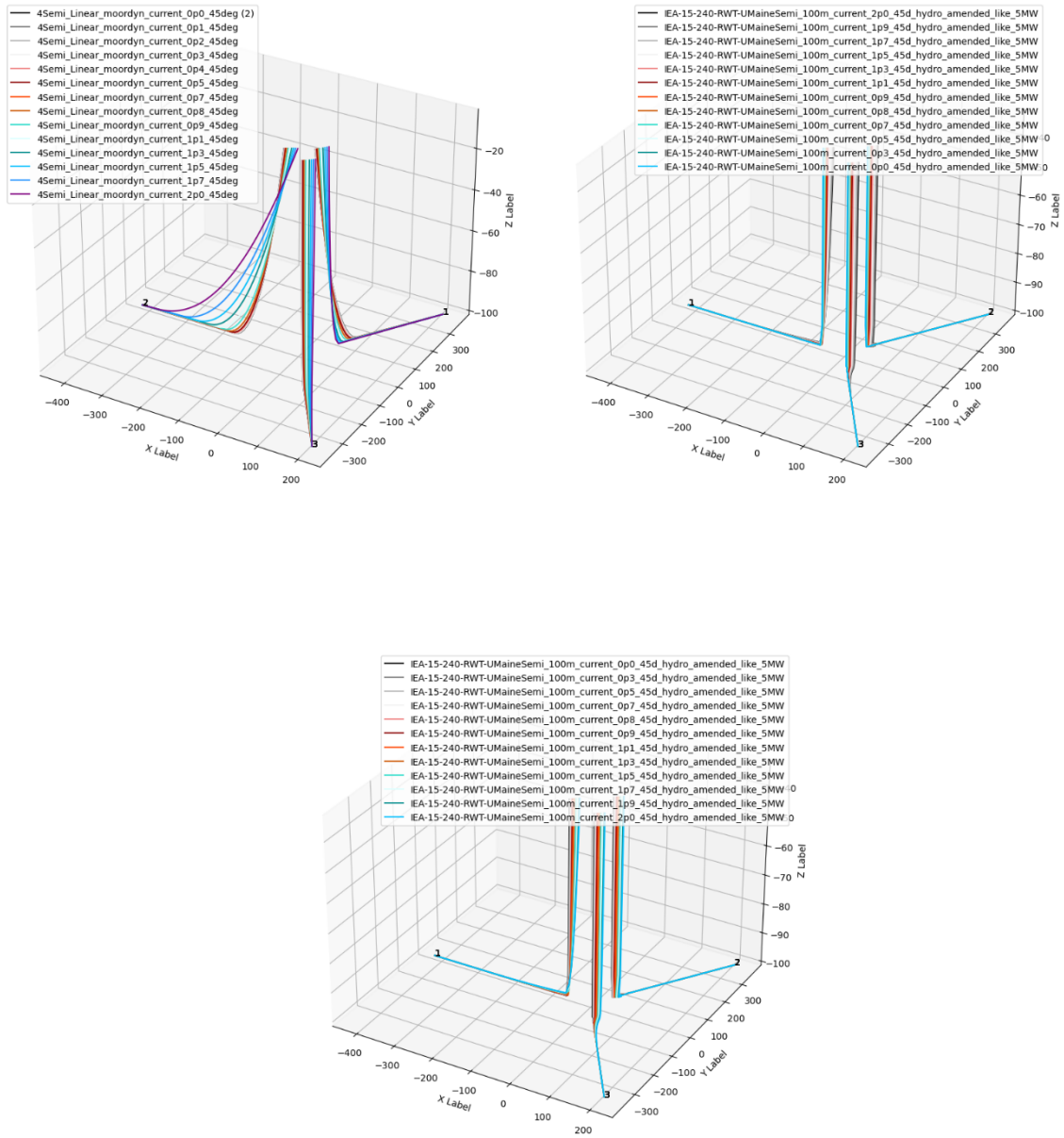

Figure 5. Overview of mooring lines position under the full range of tidal current speeds investigated with the 5 MW turbine (left) and the 15 MW turbine (right). A zero-degree current would be aligned with Y axis and moving towards positive Y. A 90-degree current would be aligned with the X axis and move towards positive X.

Under increasing current speed, results showed that the length of the upstream mooring line on the seabed decreases as it tautens, whilst the TDZ for the two downstream mooring lines increases as they slacken. For 5 MW and 15 MW turbines, when stationary, the length of the TDZ for each line was 650 m and 760 m, respectively. For the 5 MW turbine, this then varied between 441 m and 710 m depending on the position of the mooring line under different conditions. However, for the 15 MW turbine, variability under environmental parameters was greatly reduced (between 750 m and 760 m). For the larger structure, mooring lines used

here are thicker and heavier, reducing the impact from increasing current speeds, as the mooring lines require greater force to lift from the seabed (Figure 5).

Figure 6 and Figure 7 show the relationship between tidal current speed and the TDZ extent (per mooring line and combined) for the 5 MW and 15 MW structures, respectively. A range of linear and polynomial equations were fitted to the model results to identify the optimal degree to accurately link current strength with TDZ extent, with the 3rd order polynomial providing the best fit for the 5 MW structure (Figure 6). For the 15 MW structures, the variability with current magnitude suggested critical thresholds were required to move the heavier lines, depending on the orientation of the current (Figure 7). These complexities are not adequately represented with any of the equations shown. Therefore, the relationships found between the environmental conditions and resulting TDZ for the 5 MW turbine were then used to parameterise the impact on the seabed in the TELEMAC and NEMO models within the following sections.

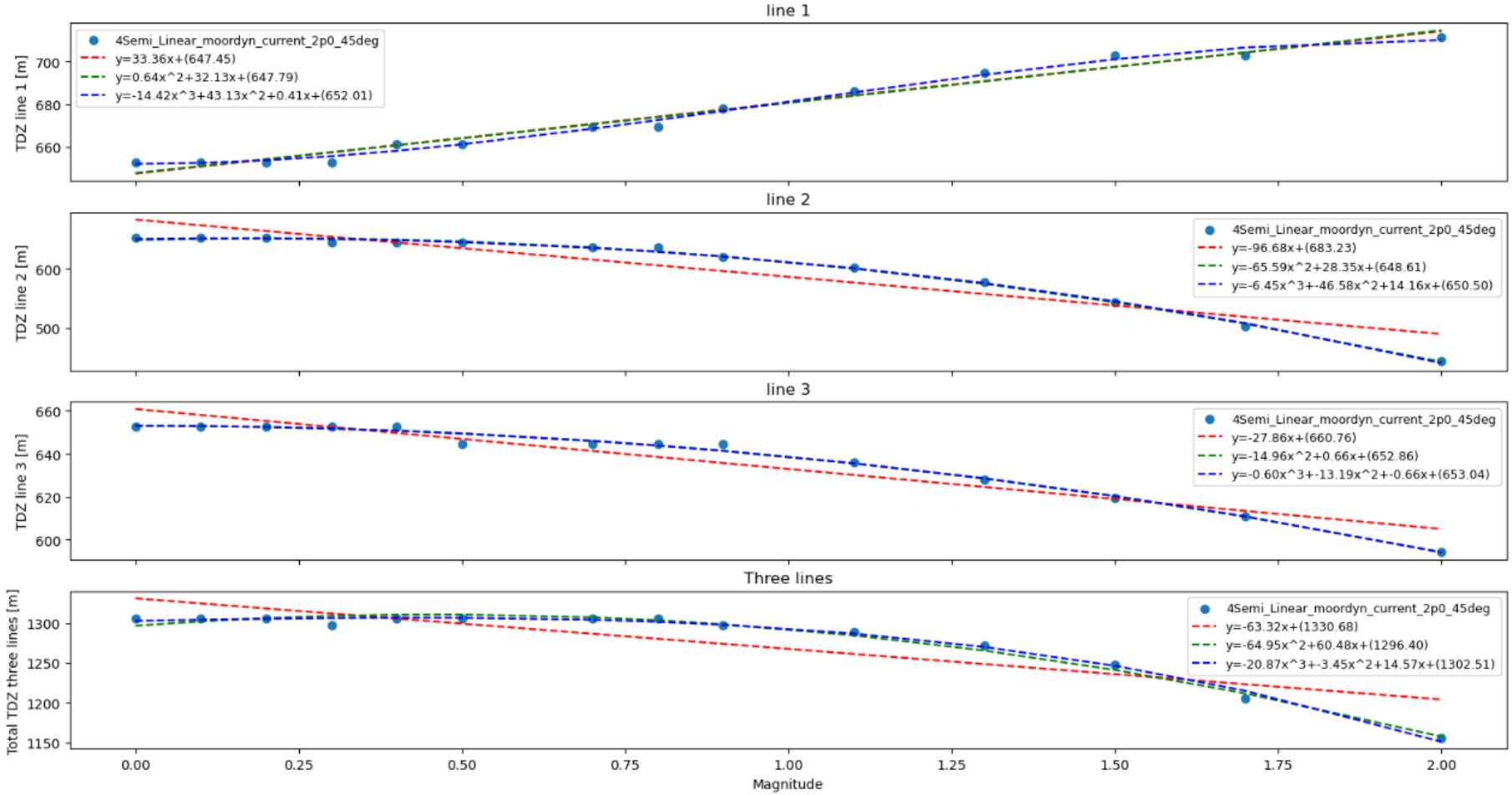

Figure 6. Relationship between tidal currents and TDZ extent per mooring line and sum of all lines, for the 5 MW turbine.

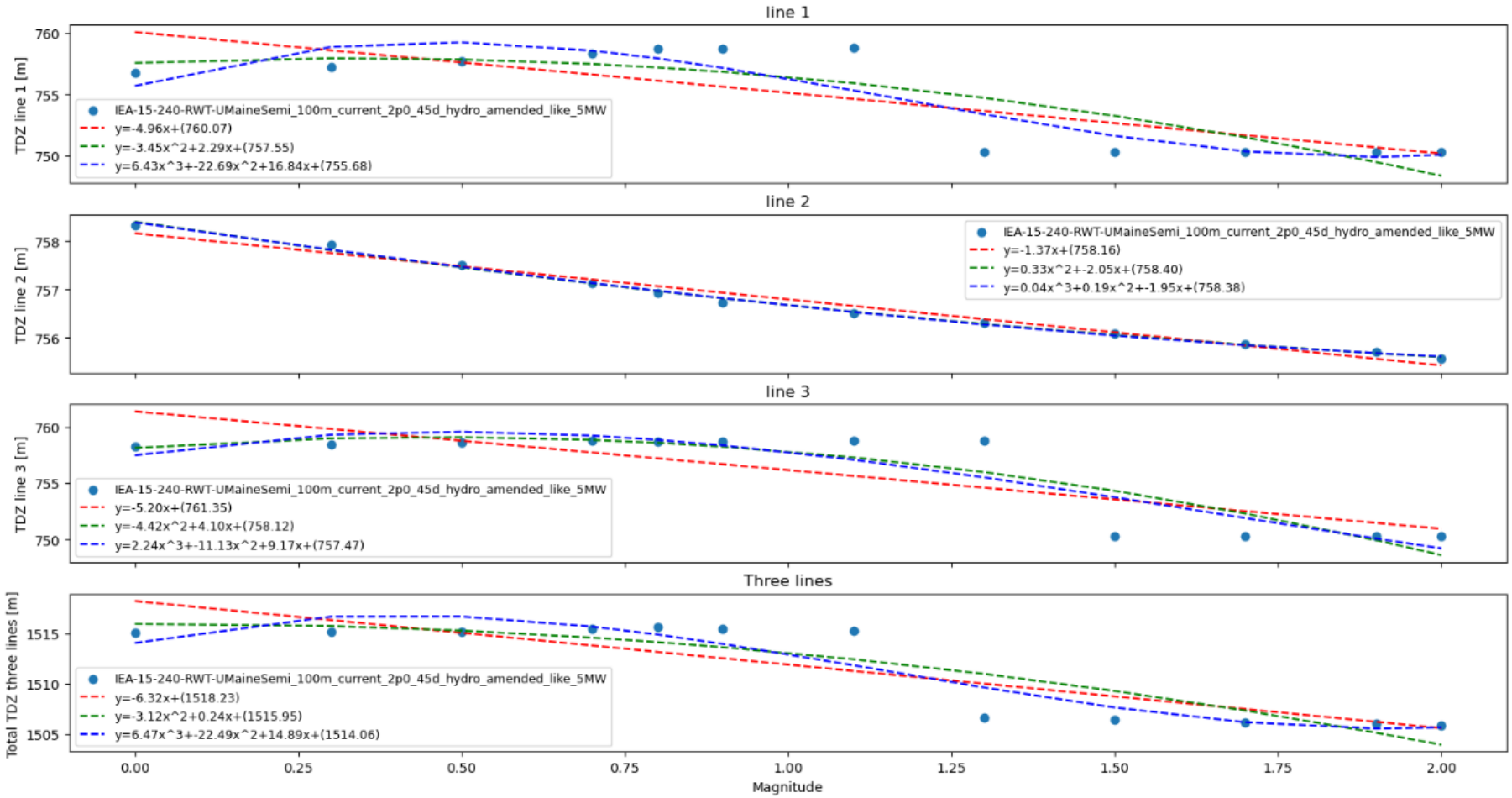

Figure 7. Relationship between tidal currents and TDZ extent per mooring line and sum of all lines, for the 15 MW turbine.

3. Wind Farm Scale Impacts

3.1 Representing Effects of Floating Wind Turbines

To assess the combined impacts of floating wind turbines on the scale of a wind farm installation and the surrounding area, this study uses the TELEMAC-3D hydrodynamic model (v8p5r0), coupled with TOMOWAC a phase resolving wave model and GAIA for sediment transport and evolution. TELEMAC is an opensource system of coupled hydro-informatics models using finite element, unstructured grid architecture to compute free-surface flow. This model was chosen as its unstructured mesh allows for varying resolution around regions of interest, to improve runtime efficiency.

While the focus of this study is the impact of the mooring lines on the sediment, there are multiple different ways that a structure is likely to interact with the marine environment (Figure 8. To investigate the physical impact of a floating wind turbine on the hydrodynamics and sediments, five different effects were then considered in the regional modelling system:

1. A localised reduction (-ve) in wind speed due to energy extraction,
2. The hydrodynamic drag (-ve) of the support structure and mooring lines,
3. An increase (+ve) in turbulence induced by the support structure and mooring lines,
4. The weight of structure acting on the free surface (+ve), and
5. A localised increase (+ve) in bed shear stress due to the mooring lines.

The wave absorbing properties of the support structure were not included in this study.

As the different effects act over different scales, each effect has been parameterised in individual areas. Figure 9 shows the delineation of the individual elements of the TELEMAC model mesh structure, for which different effects are applied, representing the floating structure, the three individual mooring lines and wake effect of the wind energy extraction. Power and telecommunication lines have been ignored at this stage. The resolution of the mesh over which the wind turbines are represented has been set at 200 m. At this stage, the impact of mesh resolution has not been investigated.

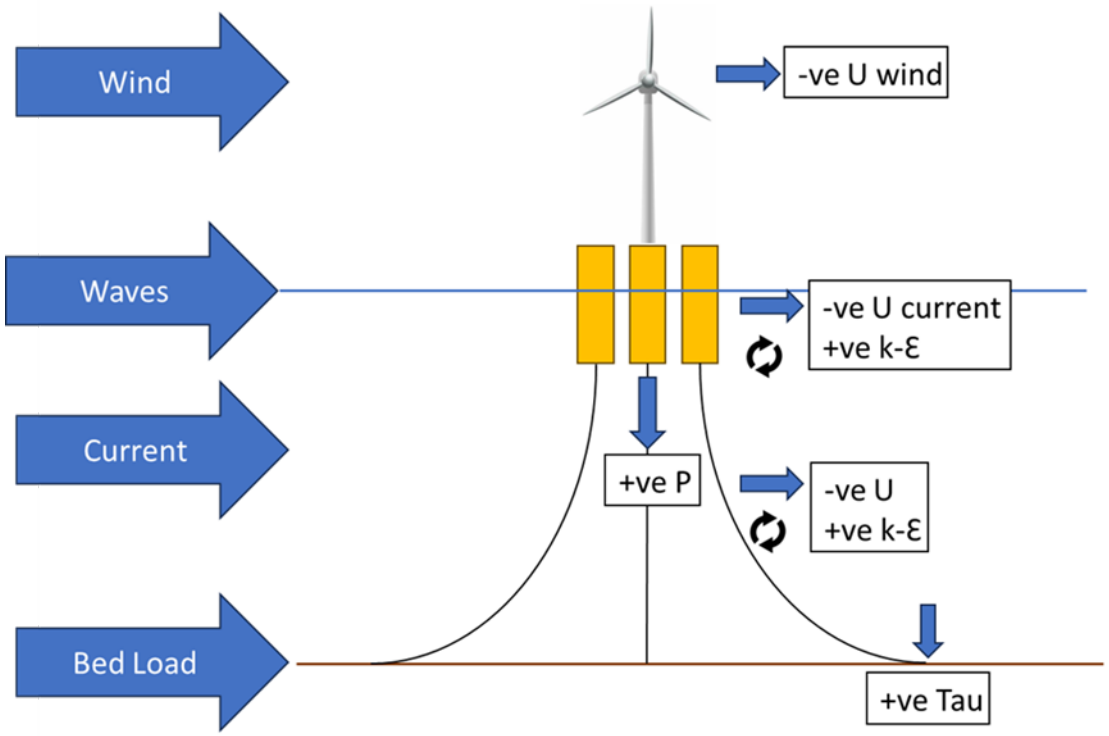

Figure 8. Different physical interactions of a floating wind turbine.

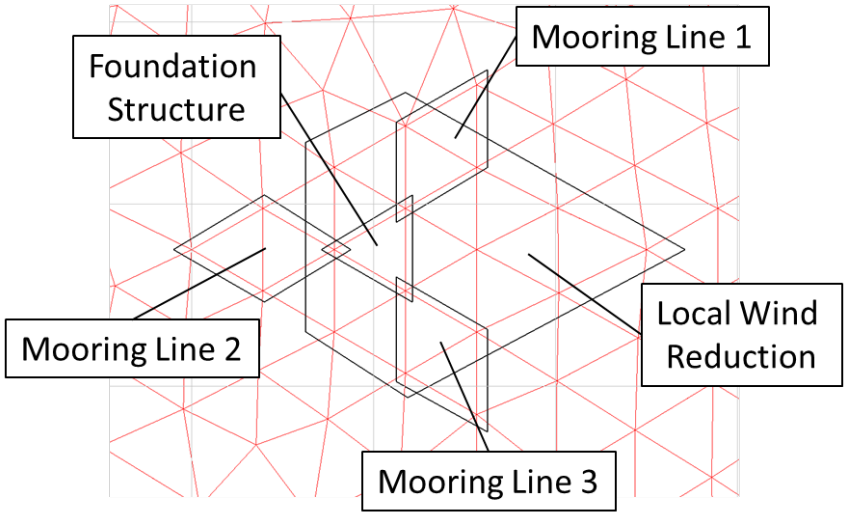

Figure 9. Discretization of wind turbine effects onto the model mesh.

3.1.1 Reduction in Wind Speed

Whilst complex fluid dynamic models investigating the propagation of wakes following energy extraction from wind turbines are possible (Sedaghatizadeh et al., 2018; Zhang and Zhao, 2020; Uchida et al., 2020), a simple approach is used here whereby a fixed proportion of the wind speed is reduced in the meteo.f subroutine, based on the peak Coefficient of Performance (Cp) of the wind turbine. For the NREL 5 MW turbine, a peak C_p = 0.48 has been used, based on the turbine specifications (Jonkman et al., 2009).

$$Wind\ Speed\_turb = (1 - C_p) \cdot Wind\ Speed \quad (1)$$

In reality, the proportion of wind energy lost would vary with the properties of the turbine blade controls, with less energy extracted at higher wind speeds to protect the wind turbine. However, the aim here is to test the proof of concept, therefore a simple approximation has been used.

3.1.2 Drag of Structure and Mooring Lines

In TELEMAC-2D, the hydrodynamic drag of a structure can be included using the dragfo.f subroutine. However, in TELEMAC-3D there is no such user subroutine. Instead, modifications have been made to the user_source.f to introduce the drag of the support structures and mooring lines on each vertical layer as a source term, as per Christiansen et al., 2023, whereby the drag is calculated as:

$$Drag\ Force = \frac{1}{2} \cdot \frac{N \times Diam}{Area} \cdot C_d \cdot \overline{U}^2 \quad (2)$$

where 'N' is the number of supports or mooring lines, 'Diam' is the diameter of the support structure or mooring line (m), 'Area' is the area of the mesh element over which the drag is applied (m^2), 'C_d' is the coefficient of drag and '$\overline{U}$' is the norm of the velocity. As both the support structures and mooring lines are approximately cylindrical, a C_d = 0.9 has been used.

Further modifications are made such that the drag of the support structure is only introduced in the top layers representing the draft of the structure, and likewise, the mooring line drag is introduced only to the lower layers below the support structure.

3.1.3 Increase in Turbulence

To introduce a new turbulence production source from the support structure and mooring lines, modifications were made to the soukep.f subroutine, as in Christiansen et al., 2023, whereby turbulence production is calculated as:

$$Prod = Prod + \left[\frac{1}{2} \cdot \frac{N \times Diam}{Area} \cdot C_d \cdot \overline{U}^3\right] \quad (3)$$

As with the drag source terms, modifications are made such that the turbulence production of the support structure is only introduced in the top layers representing the draft of the structure, and that of the mooring line is introduced only to the lower layers below the support structure. Whilst the impact of an increase in turbulence near the surface is unlikely to impact sediment transport, it has been included for future interest in potentially investigating the impact of floating wind farms in seasonally stratified waters (e.g., Dorrell et al., 2022).

3.1.4 Weight of Structure

To introduce the weight of the structure at the free surface, an additional pressure term is applied in the meteo.f subroutine, whereby atmospheric pressure is calculated as:

$$Pressure = Pressure + [\rho \cdot g \cdot draft] \quad (4)$$

where 'ρ' is water density (kg/m^3), 'g' is gravity (m/s^2), and 'draft' is the draft of the support structure (m). This is applied only at the free surface layer.

3.1.5 Increase in Bed Shear Stress

To introduce the scouring effect of the mooring line on the seabed, a localised increase in bed shear stress (τ) was parameterised in the tob_gaia.f subroutine, based on the weight of the mooring line on the seabed, and calculated as:

$$\tau = \frac{Mass\ of\ Line \times |\Delta Length\ of\ line| \times g}{Area} \quad (5)$$

where the absolute of the change in length of line (m) between the present time step and the previous is based on the third order polynomial fitted to the results of the OpenFAST simulations (Figure 6; Section 2.4). The absolute of the change in line length is used to ensure a positive value, as both a reduction and increase in the TDZ will result in scour. Whilst the effect of wind speed was investigated with OpenFAST, for simplicity and whilst developing the methodology for modelling floating wind farms, this test case focused on the response of the mooring lines to tidal currents alone. Furthermore, as the total range of change in line length was greatest for the 5 MW turbine compared to the 15 MW, the polynomials for the 5 MW turbine were used. Depending on the direction of the current in relation to the position of the mooring line, either the upstream or downstream polynomial is used. One limitation to consider therefore, is that this approach assumes the direction of the tidal currents is rectilinear. For the initial time step, the floating structure is assumed to start at the central, stationary position (velocity = 0).

3.2 Idealised Model Test Case

3.2.1 Model Set Up

To test the different interactions of the floating wind turbine, an idealised test case has been developed, representing a small-scale floating wind farm of 12 devices in an idealised channel set up. This is indicative of some of the early demonstration sites being considered (Erebus Wind Farm, 2024; White Cross Floating Wind Farm, 2024). The model domain was created using an unstructured finite element grid comprising of 3,385 nodes (6,556 elements). The model resolution is at its finest within the location of the wind farm, at 200m, extending to 500 m along the open boundaries. The channel is 43 km long and 10 km wide, with a uniform depth of 100 m. The wind farm is centred in the middle of the channel, as shown in Figure 10.

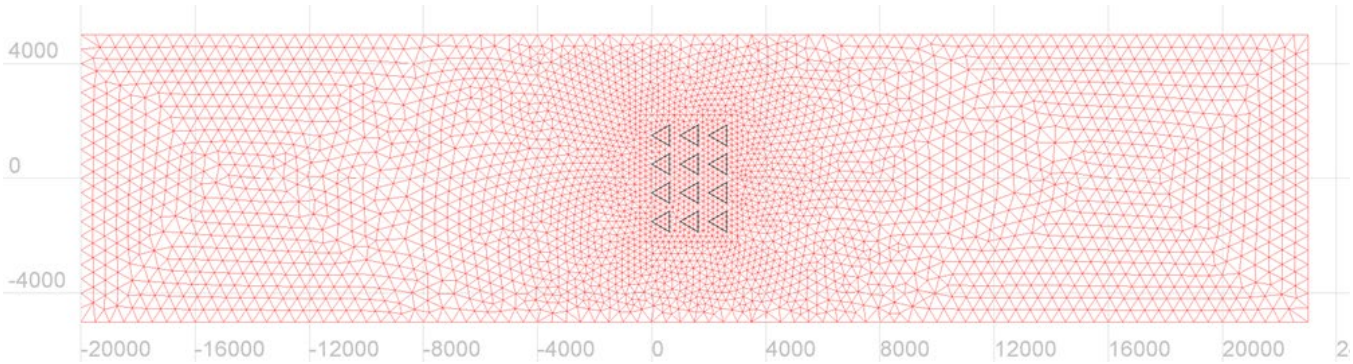

Figure 10. Idealised channel mesh. The black triangles represent the location of the individual floating wind turbines.

For the hydrodynamics, 15 vertical layers are applied at fixed depths, with 5 layers representing the top 25 m, encompassing the draft of the support structure. Another 7 layers are distributed evenly over the rest of the water column, down to 90 m where two more layers

at 2 and 5 m above the bed, help resolve the flows close to the bed. The k-epsilon turbulence model is used in both the vertical and horizontal direction.

For the sediment transport, a 2-layer bed model has been used with a 1 m thick top layer and a 10 m thick bottom layer. The active layer thickness was set to 0.5 m. For the initial testing, 5 grain sizes were used, with a uniform distribution between each size fraction, ranging evenly between 0.2 mm to 2 mm, representing the full range of the sand fraction. The uniform grain size distribution was assumed for both layers of the bed. As both waves and currents are being considered, the Bailard bedload transport formula has been used. It's worth noting that while the Soulsby bedload transport formula would have been preferable, it was not compatible with the mooring line impacts parameterisations developed here. The Soulsby formula does not utilise the bed shear stress parameter ('tob'), so this would result in no additional effect from the mooring lines within the model. For the suspended sediments, the van Rijn suspended sediment formula was used (van Rijn, 1984).

For the hydrodynamics, an idealised flowrate, resulting in a peak tidal current speed of 1 m/s through the domain, was applied to the inflow boundary, with the free surface fixed at the outflow boundary. The free surface at the inflow boundary is allowed to freely evolve to the required height to generate the required flowrate. To simulate realistic tidal patterns, a cyclic pattern ranging between 0 and 1 m/s over a 12-hour period was applied.

For the waves, a repeating 'storm' over a 99-hour period was applied, with significant wave heights (Hs) ranging sinusoidally between 0.5 m and 3 m. A constant wave period of 8 seconds was applied for the length of the simulation. This storm shape follows a similar pattern to the Environment Agency's storm surge model curves (McMillan et al., 2011). A constant wind speed of 10 m/s was applied along the model domain.

For the sediment transport, an equilibrium inflow condition was used for the bedload transport and no suspended sediments were applied at the inflow boundary. After an initial spin up period of 24 hours, the model was run for 28 days.

3.2.2 Idealised Model Results

Figure 11 shows the resulting current through the channel, demonstrating variability around the wind turbines. In the upper portion of the water column, filled by the floating structure, the current magnitude reduces by ~0.15 m/s, with a smaller 0.1 m/s increase beneath the floating structure.

Figure 12 shows the resulting cumulative bed evolution after the 28-day simulation. Within the footprint of each wind turbine, a scour pit forms at the leading front with the eroded bed material being deposited immediately downstream. This repeating pattern is localised within the footprint of the wind farm, with minimal changes detected elsewhere in the domain. The wind farm region on a whole results in a slight decrease in bedload transport, with a 2-3 cm difference in bed levels seen for ~ 4 km, in comparison to the undisturbed transport running parallel to the wind farm. However, this result may be dependent on the unidirectional flow considered within this test case. Under realistic tidal conditions, the periodic change in flow direction could remove this feature.

Figure 13 shows a time series of the bed evolution within one of the scour pits forming under a wind turbine. The rate of erosion shown in the time series can be seen to vary on the scale of the tidal current magnitude, with no variation on the scale of the wave height variation, indicating that the evolution is dominated by the tidal currents and that waves have no impact. This is not unexpected given the deep waters being simulated.

Figure 14 shows a time series of the changing proportion of the different grain sizes within the scour pit. The results are as expected, with the finer material being winnowed out first, resulting in a coarsening of the grain size distribution within the footprint of the wind turbine. Further analysis shows that for the finest grain size, 0.2 mm, the suspended sediment concentrations fall back in line with upstream undisturbed concentrations within ~7 days, with the 0.65 mm grain size, taking a further week. For the remaining fractions, none reach equilibrium during the period of the simulation. For the coarsest grain size, 2 mm, the presence of the wind farm results in continued resuspension rates above that of the undisturbed flow.

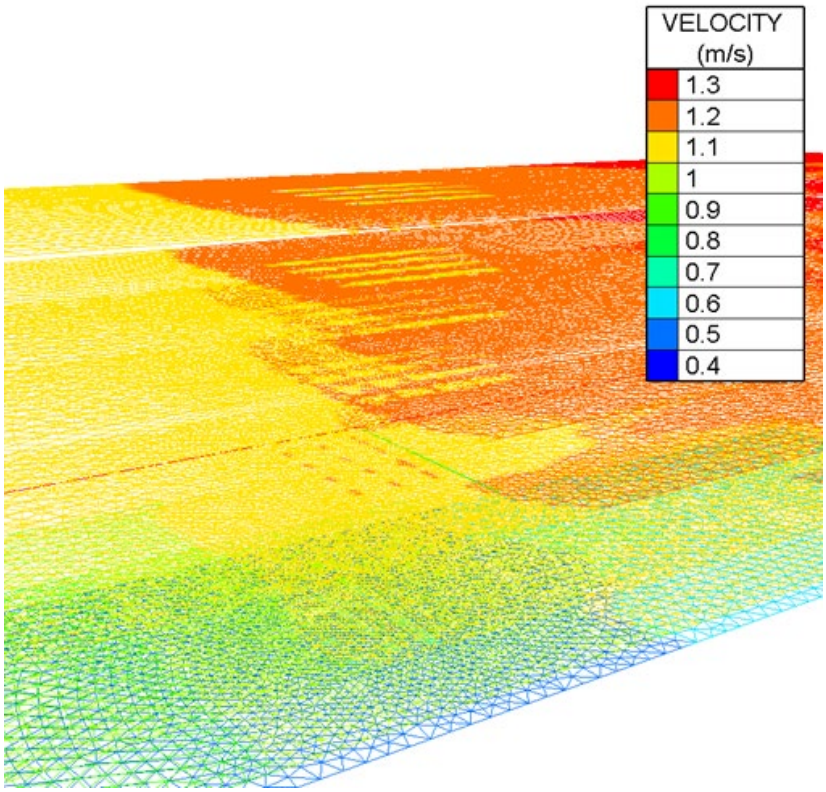

Figure 11. Instantaneous current magnitude through the wind farm for test case simulation. Some vertical layers are excluded to improve clarity in visualisation.

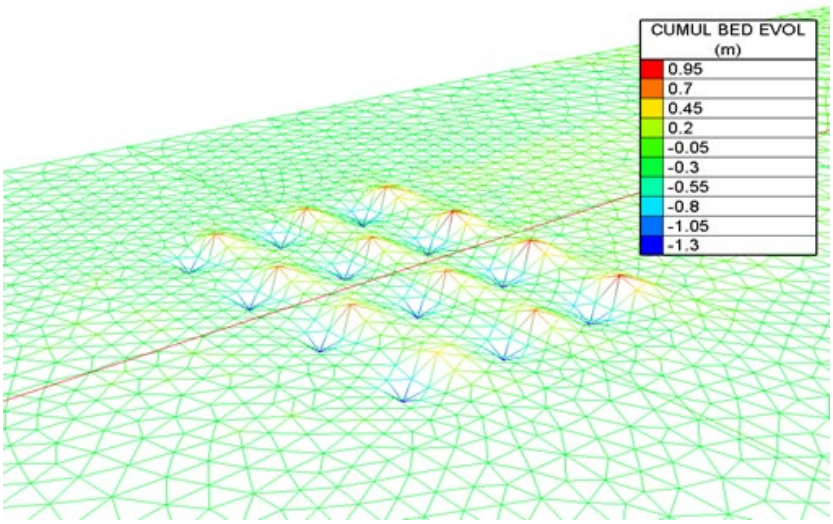

Figure 12. The cumulative bed evolution after 28-day test case simulation.

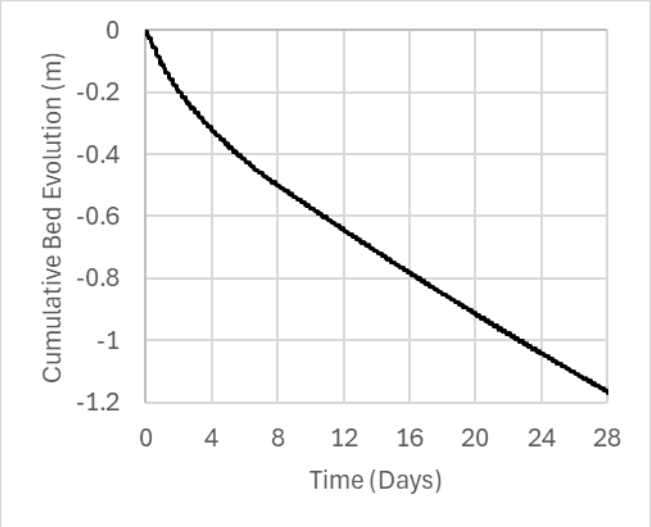

Figure 13. Time series of bed evolution within scour pit under a wind turbine.

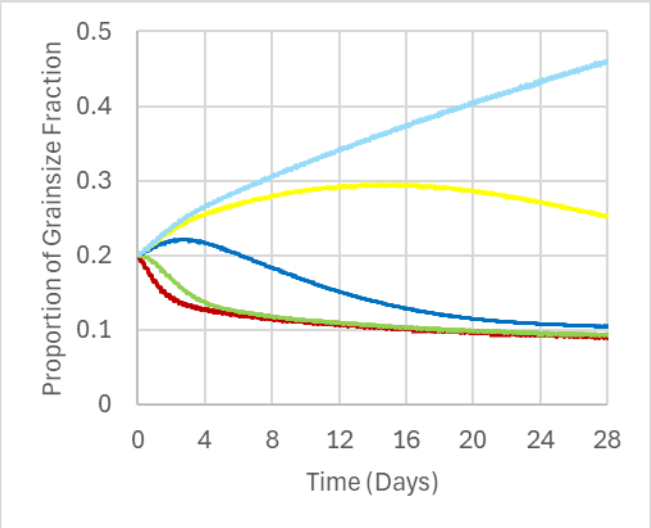

Figure 14. Change in the proportion of grain size fractions within the scour pit. Red – 0.2 mm, green – 0.65 mm, dark blue – 1.1 mm, yellow, 1.55 mm and light blue – 2 mm.

During this study, validation data has not been available to assess the speed and scale of the scour, with further work needed to obtain the necessary observations. However, the results are deemed reasonable for their intended purpose of developing an assessment methodology.

3.3 Celtic Sea Case Study

3.3.1 Model Set Up

Following successful testing with the idealised channel model, a more realistic case study was developed for a 60 MW (12 devices) wind farm in the Celtic Sea. The Celtic Sea was chosen as it is the site of several Crown Estate Offshore Wind leasing sites and proposed floating wind farm developments (Erebus Wind Farm, 2024; White Cross Floating Wind Farm, 2024). As the results of the idealised case study indicated that waves had minimal impact on the bed evolution at the depths being considered, waves were not included in the Celtic Sea case study, with the TELEMAC model being coupled to GAIA only for the sediment transport.

The model domain was again created using an unstructured finite element grid, comprising of 10,542 nodes (20,419 elements). Model resolution is finest within the location of the wind farm, at 200m, extending to ~ 10 km along the open boundaries. Figure 15 provides an overview of the model domain extent and the bathymetric depths. The model domain extends between the southern Irish coast, the southwest tip of Wales and the northern coastline of Southern England. There are three open boundaries into the Atlantic, the southern Irish Sea and the mouth of the Severn Estuary, with the hydrodynamics forced along the open maritime boundaries using 11 tidal constituents (M2, S2, N2, K2, K1, O1, P1, Q1, M4, MS4 and MN4) from the OSU TPXO European Shelf 1/12° regional model (Egbert and Svetlana, 2002). The TPXO harmonics are used to drive prescribed elevations and velocities at the open boundaries.

Bathymetry for the model was provided by the DEFRA Marine Digital Elevation Model (DEM) – 1 arc second[4]. The Marine DEM is referenced to Chart Datum. Therefore, the Marine DEM was converted from Chart Datum to Mean Sea Level using the Vertical Offshore Reference Frames (VORF) dataset (Turner et al., 2010), to ensure that bathymetry was compatible with TPXO.

A minimum water depth of 8 m was used, to ensure that no intertidal areas were present (improving model stability and run time), with depths then extending down to 128 m in the central Celtic Sea. In the location of the wind farm, depths were ~100 m. The position of the wind farm was located such that the wind turbines were situated in rectilinear flows, running east-west.

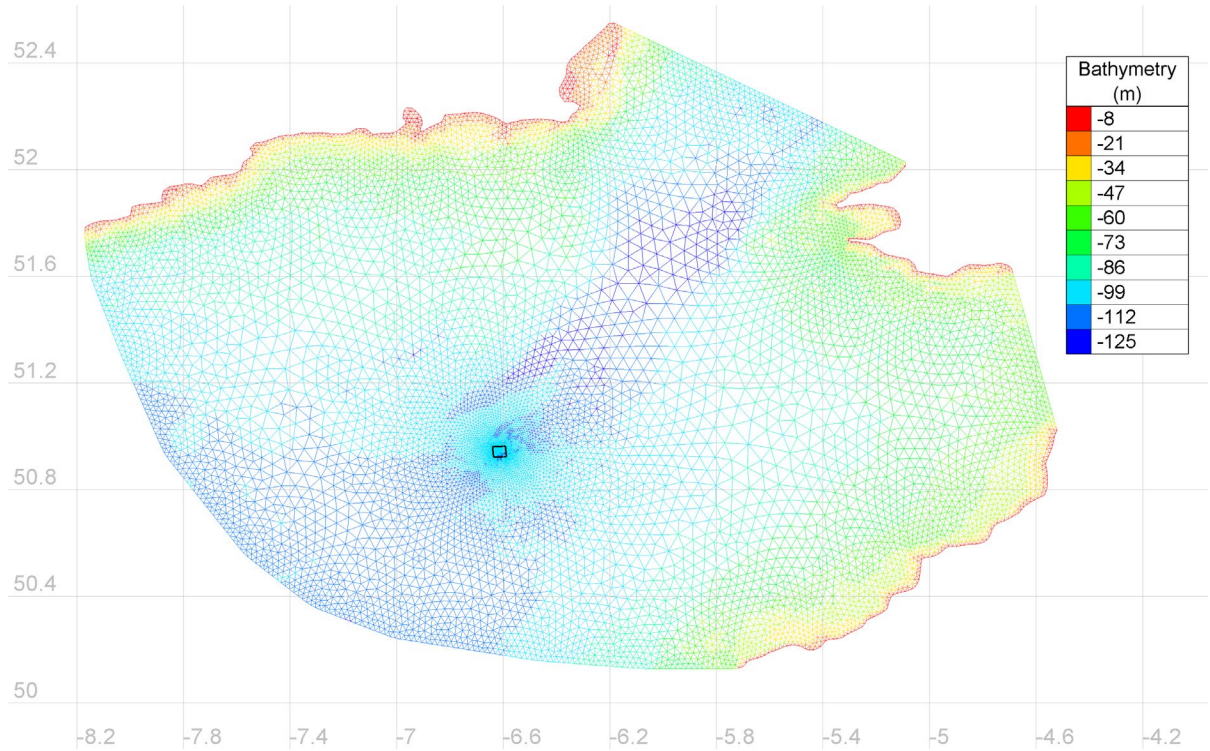

Figure 15. Bathymetric depths of Celtic Sea model domain. The black box represents the location of the floating wind farm.

[4] Defra's Marine Digital Elevation Model (DEM) - 1 arc second (south), https://www.data.gov.uk/dataset/e05d3f72-8e67-4cc0-aa2e-abb79e14243c/defra-s-marine-digital-elevation-model-dem-1-arc-second-south.

To create a realistic distribution of sediments within the domain, habitat maps were taken from the Cefas' OneBenthic catalogue[5] (Figure 16). Description of the 12 biologically based habitat classifications are described in Cooper et al., 2019, which are based on physical and biological (macrofauna) data. Each of the 12 habitat classes has an associated grain size distribution for six non-consolidated grain sizes (fine sand, medium sand, coarse sand, fine gravel, medium gravel and coarse gravel) and one mud fraction. The grain sizes used for the 7 sediment fractions were: 0.0315 mm (mud), 0.1565 mm (fine sand), 0.375 mm (medium sand), 1.25 mm (coarse sand), 5 mm (fine gravel), 12.5 mm (medium gravel) and 24 mm (coarse gravel). This provides a wider grain size distribution than that used in the idealised channel model. However, as with the idealised channel model, a two-layer bed model was used with a layer depth of 1 m and 10 m. The active layer depth was set at 0.5 m. No boundary sources for bedload transport or suspended sediments were applied.

To assess the impact of the wind farm, two scenarios were considered, a baseline run without the wind farm and one with the wind farm parameterisations, to help distinguish between the natural bed evolution and the impacts of the wind farm. For both scenarios, the model was run for a spin up period of 15 days without the wind farm, before running for a further 28 days, to represent impacts over a full spring neap cycle. Unfortunately, model instabilities on the boundary, unrelated to the presence of the wind farm, meant that both simulations were only completed for a 21-day period. We were unable to resolve these issues within the time available. However, for demonstration purposes, sufficient bed evolution had occurred to assess impact over 21 days.

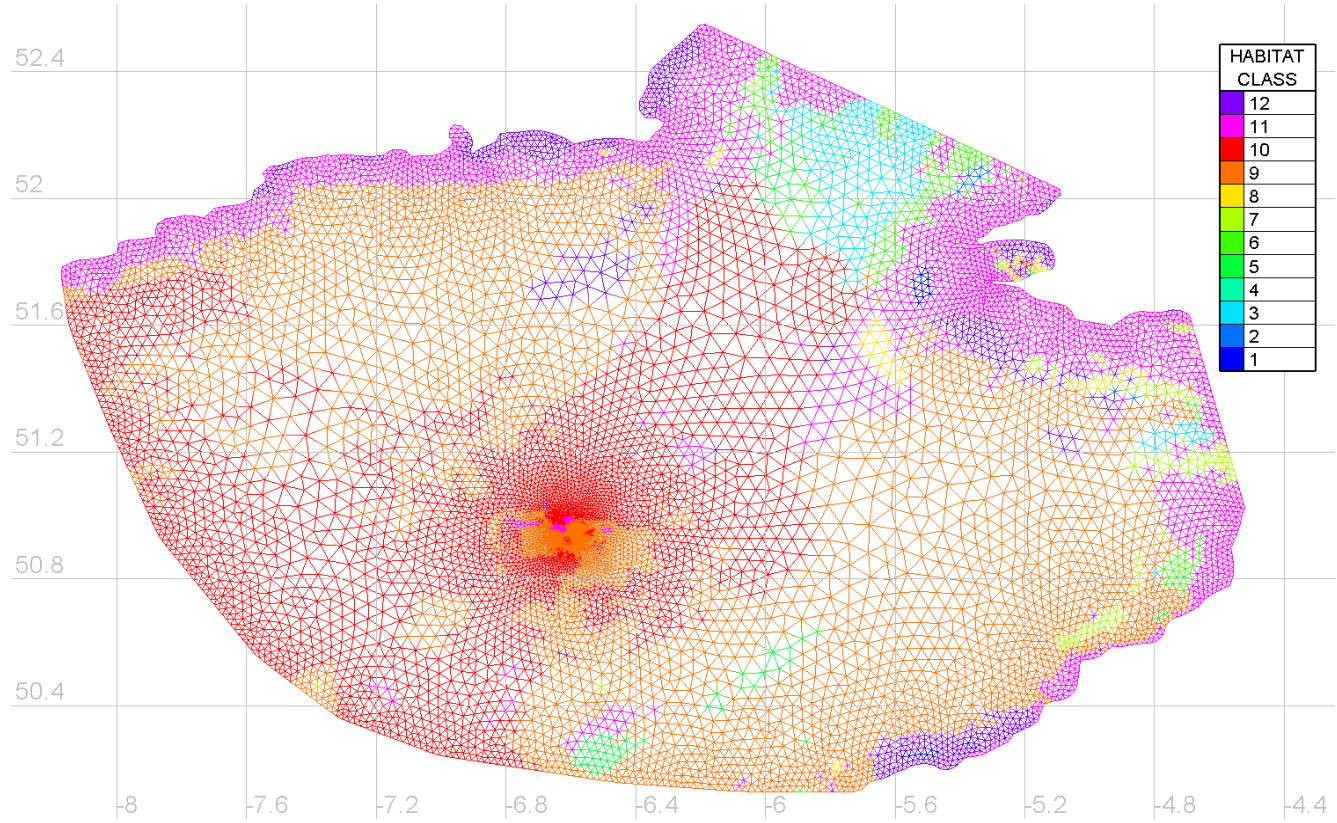

Figure 16. Habitat classification of physical and biological macrofauna assemblages used for Celtic Sea model domain, from the OneBenthic catalogue. Each habitat class has an associated grain size distribution.

[5] Cefas OneBenthic Portal, https://openscience.cefas.co.uk/.

3.3.2 Celtic Sea Case Study Results

Figure 17 shows the resulting difference in cumulative bed evolution of the two model runs (wind farm simulation and the baseline run) after the 21-day simulation. Results show a similar effect to the idealised channel model, with changes in bed evolution focussed within the wind farm. Scour pits formed under each wind turbine with scour depths ranging between 0.7 and 1.3 m. However, there was no clear signal of sediment accumulation in the lee of the wind farm, on either side.

Within the wind farm, a similar coarsening of the grain size distribution was seen. However, unlike the idealised channel model, the initial grain size distribution was not uniform, and was predominantly made up of the fine and medium sand fraction. The largest impact was seen in the medium sand fraction, reducing by 30%, with the coarse sand and fine gravel fraction increasing by 20% and 15%, respectively.

To the north of the wind farm, there is an area of erosion, with the material deposited further to the north. This erosion occurred within the first 12 hours of the simulations, so is likely a result of the initial adjustment to the inclusion of the wind farm within the model, as the flow settles between the individual turbines and the free surface stabilises from the additional pressure force of the weight of the support structure at the surface. Therefore, we expect this may be a feature of the experimental design rather than a true response to wind farm installation. To assess this further, it is recommended that future work should consider using the feature available within GAIA to pause bed evolution whilst the hydrodynamics spin up for an initial period, following the initial inclusion of the wind farm. This could mitigate the impact of initial hydrodynamic spin up, therefore allowing for more realistic development of bed load transport through the remainder of the simulation.

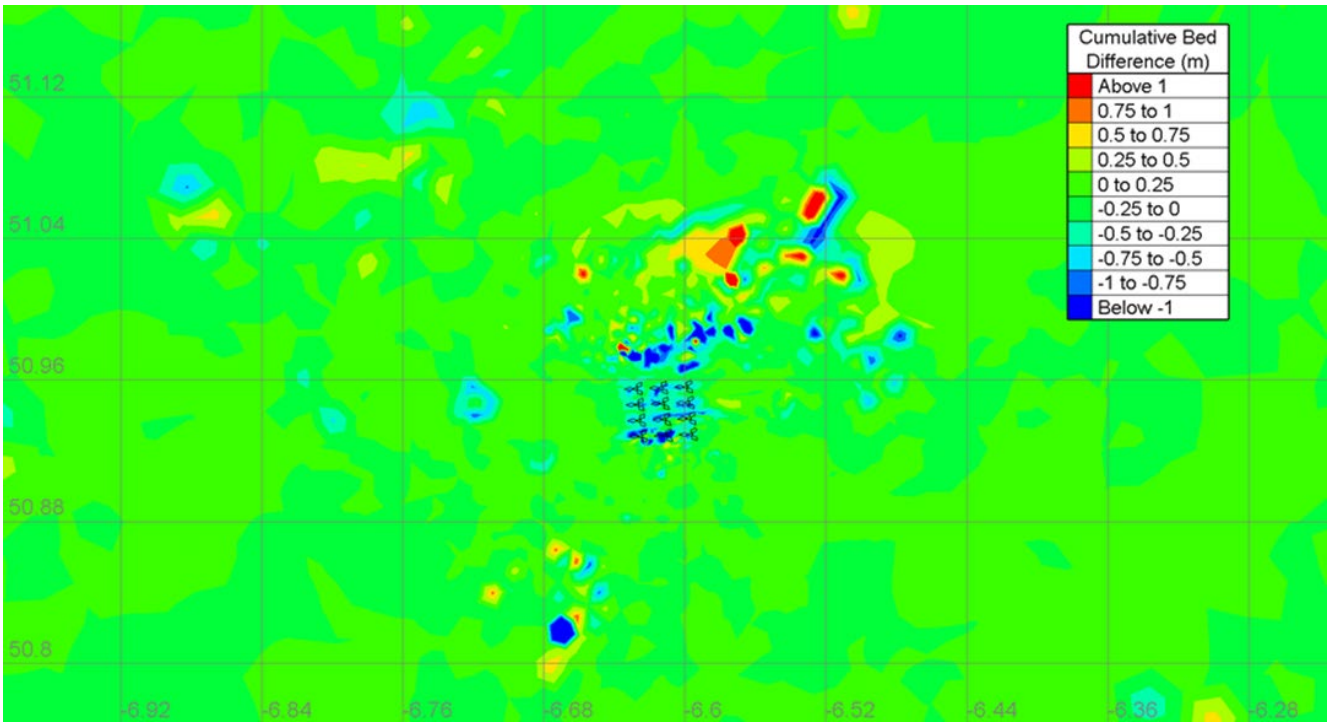

Figure 17. Difference in cumulative bed evolution with and without the wind farm after 21 days (case study minus control).

4. Shelf Scale Impacts

4.1 Model development

To investigate the potential wider shelf-scale impacts on sediment distribution, from larger scale wind farms, the NEMO hydrodynamic model was used. The configuration used here was the Atlantic Margin Model, with a horizontal resolution of 7 km (AMM7), covering the Northwest European Shelf (Figure 18; O'Dea et al., 2017). The model has up to 51 vertical levels (with terrain-following coordinates), but across shallower regions of the continental shelf, including the location of the wind farm, the water column is represented by 24 layers. This NEMO configuration has been developed by the UK Joint Marine Modelling Programme (JMMP) to provide ocean forecasting for the European North-West Shelf, and provides reanalysis of ocean conditions through EU Copernicus Marine Services Information (CMEMS, 2024). For this study, we use the same ocean and atmospheric forcing as this reanalysis product. However, we consider a free-running NEMO model (v4.0.4), without any data assimilation, coupled with a sediment transport model, through FABM (Framework for Aquatic Biogeochemical Models).

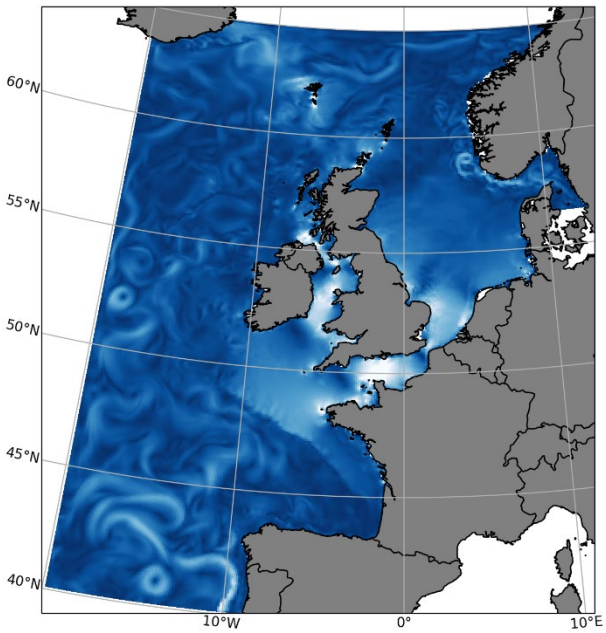

Figure 18. AMM7 model domain, shown with a snapshot of instantaneous current speeds.

The sediment transport considered here focuses on suspended particulate matter (SPM), with a single grain size used. The sediment model used was a modified version of one developed by Leibniz Institute for Baltic Sea Research Warnemünde (IOW) and distributed with FABM. Our set up used a bottom stress method as per Soulsby & Humphry (1990) and sinking method as per Soulsby (1997) and a first order resuspension method. Based on the TELEMAC modelling we wouldn't expect to see significant transport of larger sand grains at the horizontal scale of the model grid (~7km) beyond the wind farm site therefore we have concentrated on finer sediment. The sediment size used was 4 µm, as fine sediments are typical of the area. The slower settling speeds associated with this fine sediment may also lead to increased transport outside of the immediate wind farm area, enabling assessment of potential wider scale impacts. To simulate the impact of floating wind farm structures on sediment distribution, the

model development focussed purely on the impact of scour from mooring lines, to determine this impact independent from other responses within the water column. The same relationship was used between current velocity and movement of mooring lines, as implemented in the TELEMAC configuration (Section 3.1.5), with the total absolute change in touchdown length calculated at each model timestep. However, due to the coarser resolution of the model grid cells compared to the swept area of the mooring lines, the additional bed stress was considered to impact only 5% of each cell area.

To assess potential impacts of a wind farm, two simulations were then considered: a control run with no wind farm and a run with the wind farm. In the wind farm run, the floating wind farm was parameterised using the mooring line response of the 5 MW wind turbine, occupying a 3x3 grid (9 cells) in the Celtic Sea. A wind turbine density of 0.87 devices per km^2 was assumed, representing 507turbines or 2.54 GW of power capacity. Both simulations were run for 1 year[6] starting from a uniform bed sediment pool, and uniform suspended sediment provided in river input concentrations.

The code developments relating to the wind farm parameterisation, as well as the reference NEMO code and model configurations, can be found within the following Cefas code repositories:

FABM, IOW-SPM: https://github.com/CefasRepRes/Dev_fabm/releases/tag/vFLOWERS

NEMO-FABM: https://github.com/CefasRepRes/NEMO4.0-FABM/releases/tag/vFLOWERS

Model configuration: https://github.com/CefasRepRes/NEMO-FABM_Cases/releases/tag/vFLOWERS

Note that some of these repositories are currently maintained privately, internal to Cefas users. However, access may be granted to external users or developers upon request.

4.2 NEMO Results

As the model was initialised with a uniform sediment bed pool (i.e. the volume of sediment available per grid cell), there was an initial period during which the fine sediment from shallower tidally active areas redistributed within the domain. Therefore, the impact considered here focuses on differences between wind farm and control runs at the end of the simulation (Figure 19). After 1 year, there is a loss of fine sediment from the seabed within the wind farm area, and a small accumulation over the surrounding area, predominantly to the north and west of the wind farm (Figure 19a). Figure 20 shows the variability in the sediment pool within the wind farm over the course of the full 1-year simulation. Following the initial period of sediment loss at the start of the simulation, the model then demonstrates the impacts of a seasonal cycle, as well as the higher frequency tidal variability. Sediment accumulation occurs during stratified summer months, with increased loss occurring during winter months. As sediment is still being lost at the end of the year, a longer run would be needed to determine the equilibrium state of the seabed within this region.

[6] The annual run uses an existing model setup for 1993, that has previously been tested within Cefas. The configuration is currently unpublished but the report in preparation.

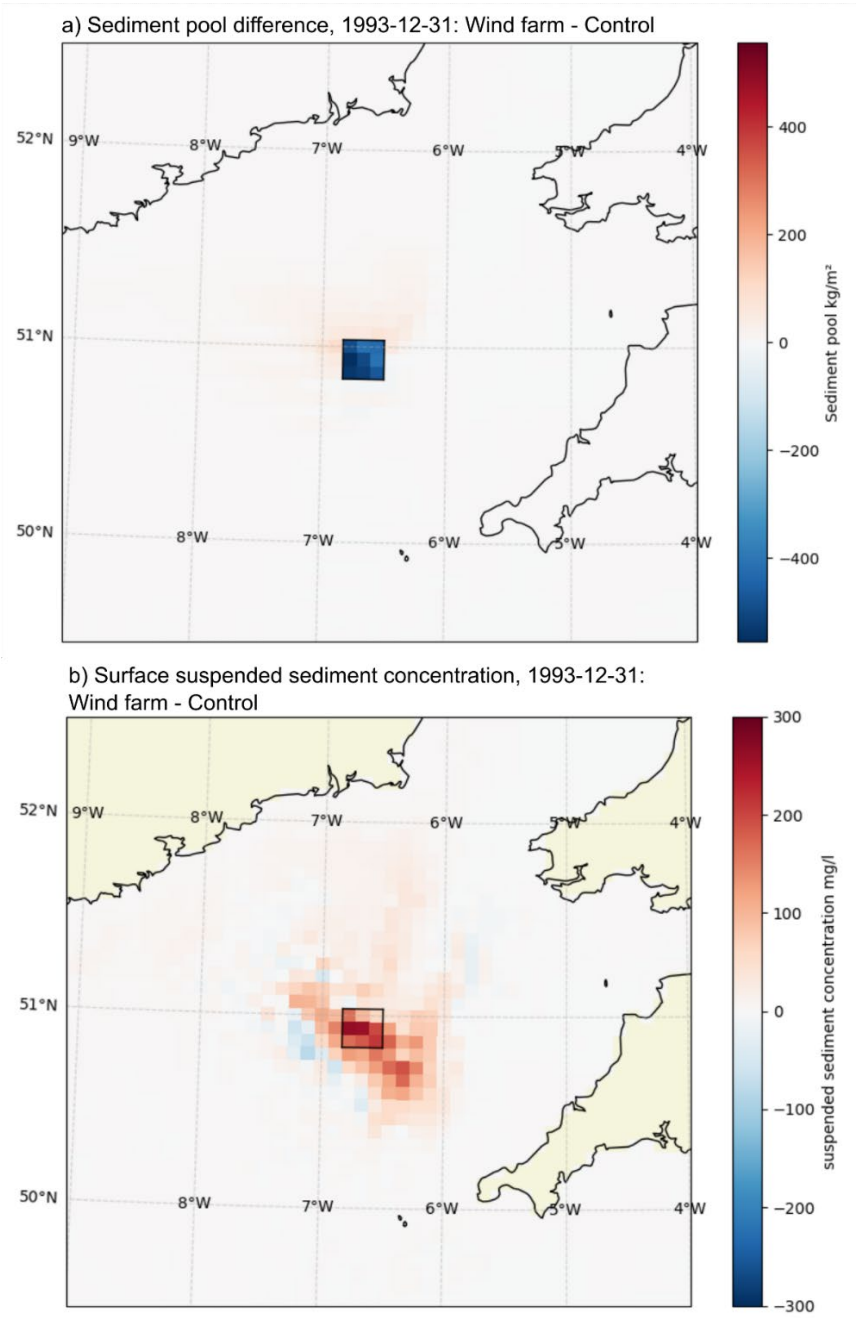

Figure 19: Difference between the wind farm minus control simulation at the end of the 1-year simulation, 31-12-1993 daily mean, for a) bed sediment pool (kg/m^2); b) suspended sediment concentration at the sea surface. Black box shows the limit of region where wind farm impacts are applied.

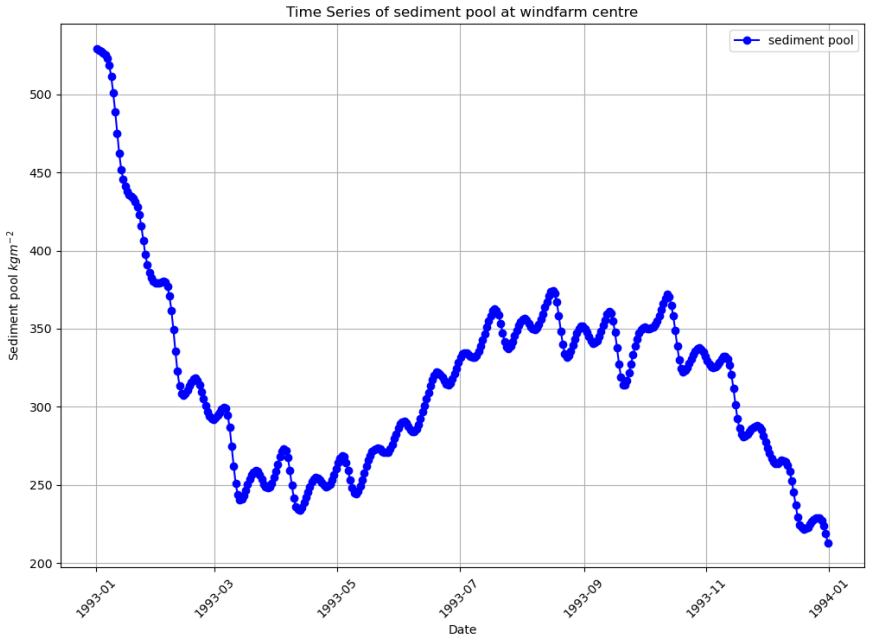

Figure 20. Time series of available sediment volume (kg/m^2) in the centre of the wind farm, over the 1-year simulation.

As sediment is lost from the seabed, there is an increase in suspended sediment at the surface in the wind farm region (Figure 19b). However, the increased suspended sediment concentration extends across a wider area, particularly to the southwest and north of the case study location. There is less increase (or potential decrease) seen to the southeast of the wind farm.

To assess how the suspended sediment concentration may vary throughout the water column, Figure 21 shows the suspended sediment concentration at the centre of the wind farm for both the control run (i.e., with no wind farm impacts) and difference with the wind farm, through the year. There is an increase in suspended sediment concentrations due to the wind farm throughout the year. However, the seasonal variability differs with depth, due to the impact of stratification. Seasonal stratification isolates suspended sediment below the thermocline during summer months (Figure 21a). The impact of the wind farm on the surface layers is then greatest during the winter months, with less impact seen above the thermocline following the onset of stratification (Figure 21b).

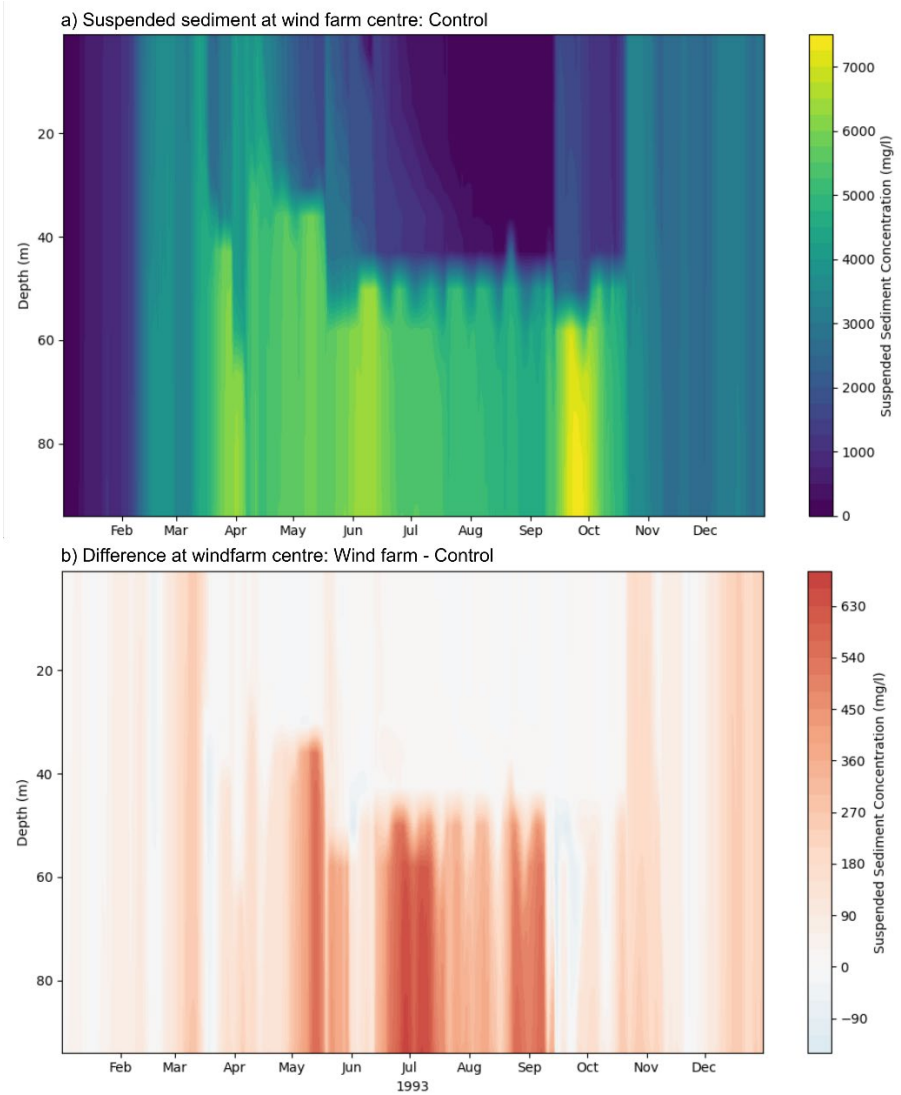

Figure 21. Suspended sediment concentrations, varying with depth and time over the year, at the centre of the wind farm, for a) control run conditions, with no wind farm impacts; b) difference between wind farm minus control.

5. Discussion

This study has focused on proof of concept, developing a methodology for future assessments of impact from floating wind structures on the seabed. A series of model simulations were used here, to consider the motion of structures, as well as impacts on different scales. Whilst the results demonstrate impacts that may be expected, further work is required to validate the responses shown within these model simulations.

The OpenFAST simulation outputs have been useful for investigating the dynamics of floating turbines under local climate conditions, allowing for predictions of mooring line movement on the seabed. However, data is lacking to crucially validate the extent of the predicted abrasion within the TDZ, as predicted within the TELEMAC simulations. The observation data required would include both the extent and shape of the scour pits beneath the structures, along with grain size distributions at different locations within the wind farm, to validate the predicted grain size coarsening and distributions. Beyond the extent of the physical impact on the

seabed, further observations of suspended sediment concentrations, throughout the water column, are also needed to validate the extent of dispersal plumes, as suggested by the NEMO-SPM simulations.

Whilst the results here have demonstrated the potential to model the impacts of floating offshore wind farms, further work is required to refine the models. For example, the NEMO model simulations only use one grain size fraction. A fine sediment was chosen here as this would travel further and therefore illustrate the potential for larger areas to be impacted. Simulations with larger grain sizes could be undertaken for comparison, although depending on sinking speed, these may not be transported significantly far outside the wind farm. In this case, the higher resolution analysis on the scale of the TELEMAC simulations may provide more useful results. Furthermore, for both the TELEMAC and NEMO simulations, longer model runs are required to 1) allow for a longer spin up period and initial seabed distribution to equalize, and 2) investigate whether scour within the wind farm reaches equilibrium, such that the resulting suspended sediment plumes become indistinguishable from background conditions. Once suitable observational data is collected a comparison should be made with these model simulations, on the understanding that the response to the wind farm structures may vary with time.

Finally, it is worth noting that the parameterisations developed here focus on 5 MW structures. Further work is needed to understand movement of larger structures (e.g., 15 MW), and also to consider potential alternative mooring designs.

6. Summary & Recommendations

This study has focussed on a demonstration case study within the Celtic Sea, to model potential impacts of floating wind turbines on the seabed, under local environmental conditions. A series of model configurations were developed to assess the motion of structures and then the impact on different scales. The Touch Down Zone (TDZ) was used as a proxy to predict the extent of the mooring line impact on the seabed, based on results from OpenFAST sensitivity tests. OpenFAST is a useful tool that allows for the adaptation of various turbine features to match a typical turbine size and specific scenarios. Results demonstrated that tidal currents had the largest impact on the seabed, followed by wind conditions, which, when strong, can make mooring lines taut (i.e. lifted from the seabed). These initial simulations considered both 5 MW and 15 MW semi-submersible structures, demonstrating that mooring line dynamics are highly dependent on structure design (i.e., size, weight, length, anchor and fairlead locations) as well as the environmental conditions (e.g., event magnitude and frequency). This study was a demonstration of the methodology using publicly available and validated model set ups, however, the code modifications are adaptable to different structures and mooring configurations. It is therefore recommended that future work should carefully consider the impact of a turbine based on the specific structures, site and local climate.

The results from the OpenFAST simulations have enabled the first implementation of a parameterisation for seabed scour, in both TELEMAC and NEMO model simulations. The TELEMAC system models the physical interactions of floating wind turbines with the marine environment via a three-way coupled TELEMAC-3D-TOMAWAC-GAIA model (for ocean, waves and sediment). Testing of the parameterisation through an idealised channel model and real-

world scenario demonstrated the proof of concept, with the flexible mesh allowing for targeted analysis around the wind farm location. These results suggest that the impact of the floating structures may be highly localised, with mooring lines resulting in local scour and coarsening of sediment grain sizes within the wind farm. Nevertheless, such changes on the seabed will have implications for marine habitats within the wind farm.

Applying the same methodology to a shelf-scale model (NEMO-SPM), has allowed for consideration of impacts to the wider region, for a chosen sediment size (4μm), over longer timescales. Results here indicate that there would be a loss of this finer sediment from the area of the wind farm over the course of a year, that may settle in the surrounding Celtic Sea. The results here show that the level of resuspension and resulting concentrations in the water column, are likely to vary through the year. However, the simulations were not long enough to determine if all fine sediment would eventually be lost, or the region reach an equilibrium state.

The methodology of combining the movements of mooring lines via engineering models, with the coupled hydrodynamic and sediment transport models, allows for assessment of impacts on seabed and therefore benthic habitats and communities. These initial simulations demonstrate potential for such models to inform spatial planning, however no observations are available to validate the results. Therefore, it is strongly recommended that in situ observations are obtained to allow for model validation, both beneath individual structures and from the surrounding marine environment. Validation with observations will enable future model development, providing confidence in the methodology. This will increase our ability to provide advice on future offshore developments.

7. References

4C Offshore Wind Map. https://map.4coffshore.com/offshorewind/. Date accessed 7th March 2024.

Allen, C., Viscelli, A., Dagher, H., Goupee, A., Gaertner, E., Abbas, N., Hall, M. and Barter, G., 2020. Definition of the UMaine VolturnUS-S reference platform developed for the IEA wind 15-megawatt offshore reference wind turbine (No. NREL/TP-5000-76773). National Renewable Energy Lab.(NREL), Golden, CO (United States); Univ. of Maine, Orono, ME (United States).

Beraud, C., Cooper, K., Musgrave, K., Rees, J., 2021. Scour around floating offshore renewable energy devices, Cefas Project Report for Defra, iv + 69 pp.one.

Christiansen, N., Carpenter, J.R., Daewel, U., Suzuki, N. and Schrum, C., 2023. The large-scale impact of anthropogenic mixing by offshore wind turbine foundations in the shallow North Sea. Frontiers in Marine Science, 10, p.1178330.

Cooper, K.M. and Barry, J., 2017. A big data approach to macrofaunal baseline assessment, monitoring and sustainable exploitation of the seabed. Scientific Reports, 7(1), p.12431.

Cooper, K.M., Bolam, S.G., Downie, A.L. and Barry, J., 2019. Biological-based habitat classification approaches promote cost-efficient monitoring: An example using seabed assemblages. Journal of Applied Ecology, 56(5), pp.1085-1098.

Dorrell, R.M., Lloyd, C.J., Lincoln, B.J., Rippeth, T.P., Taylor, J.R., Caulfield, C.C.P., Sharples, J., Polton, J.A., Scannell, B.D., Greaves, D.M., Hall, R.A. and Simpson, J.H., 2022. Anthropogenic Mixing in Seasonally Stratified Shelf Seas by Offshore Wind Farm Infrastructure. Frontiers in Marine Science, 9:830927, doi:10.3389/fmars.2022.830927

Egbert, G. D., and Erofeeva, S. Y., 2002. Efficient inverse modelling of barotropic ocean tides, Journal of Atmospheric and Oceanic Technology, 19.2: 183-204.

Erebus Floating Wind Farm, https://www.bluegemwind.com/our-projects/erebus/, Date Accessed 30th August 2024.

E.U. Copernicus Marine Services Information (CMEMS), 2024. Atlantic- European North West Shelf- Ocean Physics Reanalysis. Marine Data Store (MDS). https://doi.org/10.48670/moi-00059

Jiang, Z., 2025. Mooring design for floating wind turbines: A review, Renewable and Sustainable Energy Reviews, 212, 115231, https://doi.org/10.1016/j.rser.2024.115231.

Jonkman, J., Butterfield, S., Musial, W. and Scott, G., 2009. Definition of a 5-MW reference wind turbine for offshore system development. National Renewable Energy Laboratory, Golden. CO, Technical Report No. NREL/TP-500-38060. doi:10.2172/947422

McMillan, A., Batstone, C., Worth, D., Tawn, J., Horsburgh, K. and Lawless, M., 2011. Coastal flood boundary conditions for UK mainland and islands. Project SC060064/TR2: Design sea levels.

NREL 5MW reference turbine OpenFAST set up, https://github.com/ricklupton/OpenFAST-NREL-5MW, Date Accessed 28th August 2024.

O'Dea, E., Furner, R., Wakelin, S., Siddorn, J., While, J., Sykes, P., King, R., Holt, J., Hewitt., H, 2017. The CO5 configuration of the 7 km Atlantic Margin Model: large-scale biases and sensitivity to forcing, physics options and vertical resolution. Geoscientific Model Development, 10, pp. 2947–2969.

Robertson, A., Jonkman, J., Masciola, M., Song, H., Goupee, A., Coulling, A. and Luan, C., 2014. *Definition of the semisubmersible floating system for phase II of OC4* (No. NREL/TP-5000-60601). National Renewable Energy Lab. (NREL), Golden, CO (United States).

Sedaghatizadeh, N., Arjomandi, M., Kelso, R., Cazzolato, B. and Ghayesh, M.H., 2018. Modelling of wind turbine wake using large eddy simulation. Renewable Energy, 115, pp.1166-1176.

Sánchez, S., López-Gutiérrez, J.S., Negro, V. and Esteban, M.D., 2019. Foundations in offshore wind farms: Evolution, characteristics and range of use. Analysis of main dimensional parameters in monopile foundations. Journal of Marine Science and Engineering, 7(12), p.441.

Soulsby, R.L. and Humphery, R.L., 1990. Field observations of wave-current interaction at the sea bed. Water Wave Kinematics, Springer Netherlands, pp. 413-428

Soulsby, R., 1997. Dynamics of Marine Sands: A Manual for Practical Applications. Thomas Telford

Turner J.F., J.C. Iliffe, M.K. Ziebart, C. Wilson and K.J. Horsburgh, 2010. Interpolation of Tidal Levels in the Coastal Zone for the Creation of a Hydrographic Datum. Journal of Atmospheric and Oceanic Technology, 27(3), pp. 605-613.

Uchida, T., Taniyama, Y., Fukatani, Y., Nakano, M., Bai, Z., Yoshida, T. and Inui, M., 2020. A new wind turbine CFD modeling method based on a porous disk approach for practical wind farm design. *Energies*, *13*(12), p.3197.

UK Government Office of National Statistics, https://www.ons.gov.uk/economy/environmentalaccounts/articles/windenergyintheuk/june2021#wind-energy-data, Date Accessed 27th August 2024.

UK Research and Innovation, https://www.ukri.org/who-we-are/how-we-are-doing/research-outcomes-and-impact/epsrc/harnessing-offshore-wind/, Date Accessed 27th August 2024.

van Rijn L.C., 1984. Sediment transport - Part II: suspended load. J. of Hydraulic Division, HY11:1631–1641.

Watson, S., Moro, A., Reis, V., Baniotopoulos, C., Barth, S., Bartoli, G., Bauer, F., Boelman, E., Bosse, D., Cherubini, A., Croce, A., Fagiano, L., Fontana, M., Gambier, A., Gkoumas, K., Golightly, C., Latour, M. I., Jamieson, P., Kaldellis, J., Macdonald, A., Murphy, J., Muskulus, M., Petrini, F., Pigolotti, L., Rasmussen, F., Schild, P., Schmehl, R., Stavridou, N., Tande, J., Taylor, N., Telsnig, T., Wiser, R., 2019. Future emerging technologies in the wind power sector: A European perspective, Renewable and Sustainable Energy Reviews, 113, 109270, https://doi.org/10.1016/j.rser.2019.109270.

White Cross Floating Wind Farm, https://whitecrossoffshorewind.com/, Date Accessed 30th August 2024.

Zhang, J. and Zhao, X., 2020. A novel dynamic wind farm wake model based on deep learning. Applied Energy, 277, p.115552.